Automated Triage Radiation Biodosimetry: Integrating Imaging Flow Cytometry with High-Throughput Robotics to Perform the Cytokinesis-Block Micronucleus Assay

Authors: Wang, Qi, Rodrigues, Matthew A., Repin, Mikhail, Pampou, Sergey, Beaton-Green, Lindsay A., et al.

Automated Triage Radiation Biodosimetry: Integrating Imaging Flow Cytometry with High-Throughput Robotics to Perform the Cytokinesis-Block Micronucleus Assay

Qi Wang,[a,1,2] Matthew A. Rodrigues,[c] Mikhail Repin,[a] Sergey Pampou,[b] Lindsay A. Beaton-Green,[d] Jay Perrier,[a] Guy Garty,[a] David J. Brenner,[a] Helen C. Turner[a] and Ruth C. Wilkins[d]

[a] Center for Radiological Research and [b] Columbia Genome Center High-Throughput Screening Facility, Columbia University Medical Center, New York, New York 10032; [c] MilliporeSigma, Seattle, Washington, 98119; and [d] Consumer and Clinical Radiation Protection Bureau, Health Canada, Ottawa K1A 1C1, Canada

Wang, Q., Rodrigues, M. A., Repin, M., Pampou, S., Beaton-Green, L. A., Perrier, J., Garty, G., Brenner, D. J., Turner, H. C. and Wilkins, R. C. Automated Triage Radiation Biodosimetry: Integrating Imaging Flow Cytometry with High-Throughput Robotics to Perform the Cytokinesis-Block Micronucleus Assay. *Radiat. Res*. 191, 342–351 (2019).

The cytokinesis-block micronucleus (CBMN) assay has become a fully-validated and standardized method for radiation biodosimetry. The assay is typically performed using microscopy, which is labor intensive, time consuming and impractical after a large-scale radiological/nuclear event. Imaging flow cytometry (IFC), which combines the statistical power of traditional flow cytometry with the sensitivity and specificity of microscopy, has been recently used to perform the CBMN assay. Since this technology is capable of automated sample acquisition and multi-file analysis, we have integrated IFC into our Rapid Automated Biodosimetry Technology (RABiT-II). Assay development and optimization studies were designed to increase the yield of binucleated cells (BNCs), and improve data acquisition and analysis templates to increase the speed and accuracy of image analysis. Human peripheral blood samples were exposed *ex vivo* with up to 4 Gy of γ rays at a dose rate of 0.73 Gy/min. After irradiation, samples were transferred to microtubes (total volume of 1 ml including blood and media) and organized into a standard 8 × 12 plate format. Sample processing methods were modified by increasing the blood-to-media ratio, adding hypotonic solution prior to cell fixation and optimizing nuclear DRAQ5 staining, leading to an increase of 81% in BNC yield. Modification of the imaging processing algorithms within IFC software also improved BNC and MN identification, and reduced the average time of image analysis by 78%. Finally, 50 μl of irradiated whole blood was cultured with 200 μl of media in 96-well plates. All sample processing steps were performed automatically using the RABiT-II cell::explorer robotic system adopting the optimized IFC-CBMN assay protocol. The results presented here detail a novel, high-throughput RABiT-IFC CBMN assay that possesses the potential to increase capacity for triage biodosimetry during a large-scale radiological/nuclear event. © 2019 by Radiation Research Society

INTRODUCTION

The cytokinesis-block micronucleus (CBMN) assay is a well-established biodosimetry technique for assessing genetic damage after a radiation accident or event (*1, 2*). The CBMN assay quantifies the frequency of micronuclei (MN) in binucleated cells (BNCs) derived from human peripheral lymphocytes (*1, 3, 4*). Micronuclei are formed from whole chromosomes or chromosome fragments that lag behind during the metaphase-anaphase transition and are not included inside one of the two main nuclei after karyokinesis. Instead, MN form into small, rounded bodies surrounded by their own nuclear envelope and can persist for up to one year after their generation (*5*). The CBMN assay is traditionally scored by manual microscopy, which is labor intensive, time consuming and subject to scorer variability.

After a radiation accident or event involving large numbers of casualties, there is an urgent need to obtain accurate dose estimates as quickly as possible so that health care providers can determine the proper treatment course. While many attempts have been made recently to automate or semi-automate image analysis, currently the CBMN assay still relies on manual slide preparation for microscope-based analysis (*6–8*).

Over the past decade, the Columbia Center for High-Throughput Minimally-Invasive Radiation Biodosimetry (New York, NY) has developed the Rapid Automated Biodosimetry Tool (RABiT) based on custom-built robotic platforms (*9*). The RABiT is designed to be a completely automated, ultra-high-throughput, robotically-based biodosimetry workstation that can analyze fingerstick-derived

---

blood samples for retrospective biodosimetry or to identify individuals exposed above or below a cut-off dose (4, 10). High-throughput is achieved through purpose-built robotics, sample handling in 96-well format and innovations in high-speed imaging and analysis. RABiT biodosimetry assays have been developed for protocols that include the CBMN assay (11, 12), the γ-H2AX assay (13–15) and the dicentric chromosome assay (16). The philosophy of the new generation of the RABiT (RABiT-II) is to make use of already deployed and commercially available automated biotech systems to perform high-throughput biodosimetry (17). Although the RABiT-II has greatly improved the throughput of biomarker assays, protocols are still limited by the requirement to transfer the harvested samples to slides, or data acquisition from imaging plates, both of which represent a bottleneck for rapid sample processing and image acquisition. Thus, there is a need to improve the ''time to result'' by minimizing the time required for sample processing and image analysis.

Imaging flow cytometry (IFC) is relatively new technology that has been developed to combine the statistical power of traditional flow cytometry with the sensitivity and specificity of microscopy. Similar to traditional flow cytometry, cells are labeled with fluorescent dyes and are loaded, in suspension, into the ImageStream®X (ISX) imaging flow cytometer. Cells are hydrodynamically focused into the center of a flow cell cuvette and orthogonally illuminated by a Brightfield (BF) light-emitting diode, side scatter laser and lasers to generate fluorescent photons that are collected by a charge-coupled device camera. The ISX simultaneously captures fluorescent and BF images at a rate of more than 1,000 cells/s, enabling several different structures within the cell to be analyzed (18).

Recently, the CBMN assay has been adapted to an IFC-based method for use in genetic toxicology testing (19, 20) and triage radiation biodosimetry (21–25). These methods demonstrated that cellular images of both the cytoplasm and fluorescence-labeled nuclei and MN could be captured at higher throughput than other methods used to perform the assay. All samples were run in suspension on the ISX and all captured imagery was stored in dose-specific data files, eliminating the need to make microscope slides (21). BNCs and MN were automatically identified in the Image Data Exploration and Analysis Software (IDEAS®) by using mathematical algorithms to implement BNC/MN scoring criteria (2, 26). The IFC-based version of the CBMN assay has been shown to automatically score more BNCs than can be scored using manual microscopy in a fraction of the time, which enhances the statistical robustness and speed of the assay (19). For radiation biodosimetry, dose-response calibration curves from whole blood samples exposed to 0–4 Gy of X rays were created to quantify the frequency of MN per BNC (24). The method was optimized and validated using blinded samples and was shown to generate dose estimation within ±0.5 Gy of the true dose (24, 25).

The goal of this study was to integrate the IFC-CBMN assay protocol into the RABiT-II to achieve an automated system that would improve throughput and efficiency for radiation biodosimetry in a mass casualty scenario. Assay development and optimization studies were designed to: 1. Adapt the IFC-based CBMN assay protocol for small blood volumes in 2-dimensional (2D) Matrix™ microtubes, organized into a standard 8×12 plate format; 2. Optimize sample processing to increase the yield of BNCs per culture volume; and 3. Increase the speed of data acquisition and improve the accuracy of image analysis. The results presented in this article show dose-response calibration curves obtained from just 50 μl of whole blood, which was exposed to 0–4 Gy of γ rays using our novel high-throughput RABiT-IFC CBMN assay.

DEVELOPMENT OF THE IFC-BASED CBMN ASSAY PROTOCOL FOR SMALL BLOOD VOLUMES

Blood Collection and Irradiation

Blood was collected by venipuncture from healthy adult donors (between the ages of 27–48 years) with informed consent and with approval by Columbia University's Research Ethics Board (approved IRB protocol IRB-AAAE-2671) in 5-ml lithium-heparinized Vacutainer® tubes (BD Vacutainer™, Franklin Lakes, NJ). All donors were non-smokers in relatively good health at the time of donation with no obvious illnesses such as colds, flu or infections and no known exposures to medical ionizing radiation within the last 12 months. Aliquots of blood samples (1 ml) were dispensed into 15-ml conical bottom tubes (Santa Cruz Biotechnology® Inc., Dallas, TX) and transported to a Gammacell® 40 ^{137}cesium (^{137}Cs) irradiator (Atomic Energy of Canada Ltd., Chalk River, Canada). The blood sample tubes were placed on their side in the middle of the chamber and exposed to 0 (control), 1.0, 2.0, 3.0 or 4.0 Gy of γ rays at a dose rate of 0.73 Gy/min. The ^{137}Cs irradiator is calibrated annually with TLDs and homogeneity of exposure across the sample volume was verified using EBT3 Gafchromic™ film with less than 2% variation within the sample (Ashland Advanced Materials, Bridgewater, NJ).

Small Volume CBMN Assay Protocol

Aliquots of 100 μl from the irradiated blood samples were added to 1.4 ml 2D Matrix microtubes (Thermo Scientific™, Waltham, MA) containing 900 μl PB-MAX karyotyping media (Life Technologies, Grand Island, NY). Each microtube was mixed five times using a 1.2-ml multi-channel electronic pipet (Eppendorf Inc., Westbury, NY or Thermo Scientific). The rack containing microtubes was placed into an incubator at 37°C, 5% CO_2. After 24 h of incubation, cytochalasin-B (Cyto-B; Sigma-Aldrich®, St. Louis, MO) was added to cultures at a final concentration of 6 μg/ml to block cytokinesis of proliferating lymphocytes. After an additional 44 h of incubation, the samples were
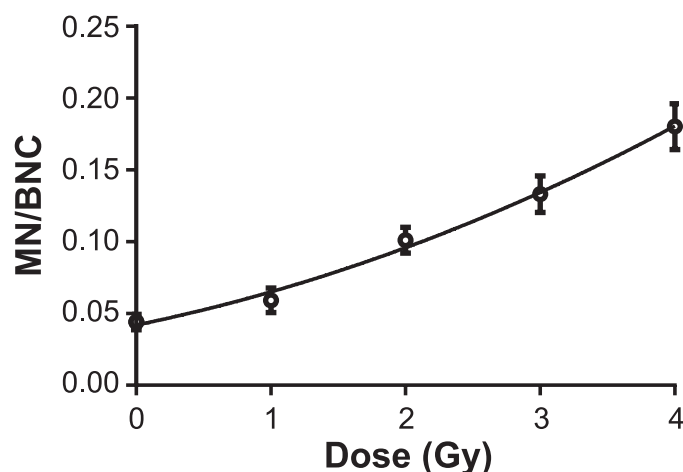
FIG. 1. Dose-response calibration curve representing the average rate of micronuclei (MN) per binucleated cell (BNC) in lymphocytes from 100-µl whole blood samples, which were collected from four healthy donors and *ex vivo* exposed to 0 to 4 Gy. Error bars represent the standard error of the mean.

harvested and the microtube plates were spun down before the supernatant was removed.

Samples were then resuspended in 900 µl FACS™ Lysing Solution for 2 min (FLS; BD Biosciences, Franklin Lakes, NJ) and spun down. The cells were resuspended in 950 µl FLS and incubated for 13 min, and then spun down again. Each sample was then washed twice with 950 µl 1× phosphate buffered saline (PBS; Gibco®, Gaithersburg, MD) and resuspended in a final volume of 25 µl PBS. All steps in the procedure were performed at room temperature and microtubes in racks were spun at 250*g* for 3 min. Finally, DRAQ5 (eBioscience, San Diego, CA) was added to the sample at a final concentration of 20 µ*M* and incubated at room temperature for a minimum of 5 min.

Data Acquisition and Analysis on the ISX and IDEAS

All samples in suspension were run on the ISX MKII system (MilliporeSigma, Seattle, WA) at 40× magnification with the 488-nm laser set to the maximum 200 mW. BF images were collected in channel 1 while DRAQ5 images

were collected in channel 5. All other channels were disabled during data collection. Data were collected using the ISX INSPIRE® software with only the Area feature applied. Events with area less than 100 pixels (25 µm^2) were gated out to minimize the collection of small debris. A total of up to 200,000 events were collected per sample and each data file typically took approximately 13 min to acquire, on average.

All data were analyzed based on the gating strategy developed in the IDEAS software package described elsewhere (*24*). Briefly, the analysis identifies BNCs that possess nuclei of high circular morphology, similar areas and DRAQ5 intensities, and with sufficient spatial separation (i.e., not overlapping). Once the final BNC population was obtained, MN within the BNCs were automatically identified and enumerated. The analysis template was applied to all data files and automatically batch processed, which enabled the number of BNCs and MN per file to be extracted and exported to Office 365® Microsoft Excel for analysis.

Dose-Response Calibration Curve

All calibration curves were generated using GraphPad Prism version 6 (La Jolla, CA), and fitted with a non-linear regression quadratic equation of the form:

$$Y = c + \alpha D + \beta D^2,$$

where *Y* is the number of MN per BNC, *D* is the dose, *c* is a constant, and α and β are constants corresponding to the linear and quadratic components of the dose, respectively. Goodness of fit (R^2) of the calibration curve was tested. Figure 1 shows the average dose-response calibration curve obtained from 100-µl whole blood samples from four healthy donors. Coefficients for all dose-response calibration curves are shown in Table 1. It can be seen that MN frequency increases according to a linear-quadratic dependence with dose as expected from previously reported results (*23, 24*). The average number of BNCs from all samples was 509 at 0 Gy and 250 at 4 Gy, sufficient for triage biodosimetry (*27, 28*).

TABLE 1
Coefficient Values Calculated for each Linear-Quadratic Fit and Goodness of Fit (R^2) from each Calibration Curve for Figs. 1–4

|	$\beta \pm$ SE	$\alpha \pm$ SE	$c \pm$ SE	R^2
Fig. 1	$(3.0 \pm 3.5) \times 10^3$	$(32.8 \pm 4.1) \times 10^3$	$(30.5 \pm 8.5) \times 10^3$	0.86
Fig. 2, blood-to-media ratio 1:9	$(3.0 \pm 3.5) \times 10^3$	$(32.8 \pm 4.1) \times 10^3$	$(30.5 \pm 8.5) \times 10^3$	0.86
Fig. 2, blood-to-media ratio 2:8	$(0.9 \pm 3.6) \times 10^3$	$(31.5 \pm 4.3) \times 10^3$	$(108.3 \pm 9.6) \times 10^3$	0.70
Fig. 3, KCl + FLS	$(10.0 \pm 2.7) \times 10^3$	$(3.8 \pm 3.1) \times 10^3$	$(67.0 \pm 7.0) \times 10^3$	0.87
Fig. 3, FLS only	$(0.9 \pm 3.6) \times 10^3$	$(31.5 \pm 4.3) \times 10^3$	$(108.3 \pm 9.6) \times 10^3$	0.70
Fig. 4, 10 µ*M*	$(1.3 \pm 6.2) \times 10^3$	$(27.8 \pm 7.4) \times 10^3$	$(1.2 \pm 6.2) \times 10^3$	0.39
Fig. 4, 20 µ*M*	$(10.0 \pm 2.4) \times 10^3$	$(38.2 \pm 2.9) \times 10^3$	$(67.0 \pm 6.4) \times 10^3$	0.90
Fig. 4, 50 µ*M*	$(5.3 \pm 6.8) \times 10^3$	$(31.0 \pm 8.0) \times 10^3$	$(94.8 \pm 17.8) \times 10^3$	0.48
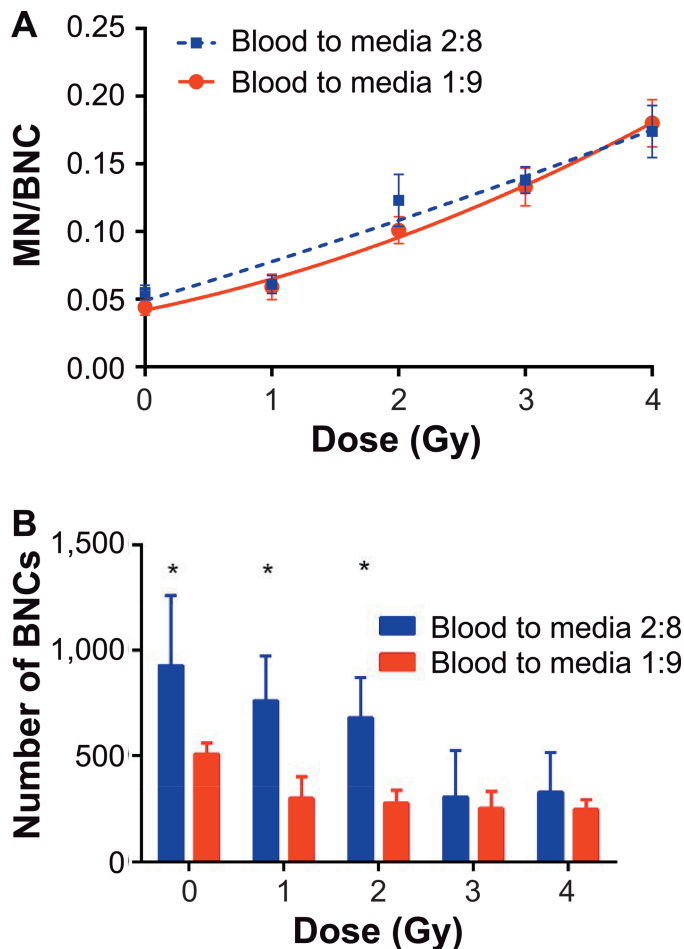
FIG. 2. Optimization of blood-to-media ratio. Panel A: Dose-response calibration curves indicating a similar increase in MN frequency for both the 1:9 and 2:8 blood-to-media ratios. Panel B: The average number of BNCs scored for the 1:9 and 2:8 blood-to-media ratios. All data points represent the average of four donors and error bars represent the standard error of the mean. Statistical significance of BNCs between the two groups was examined by the Wilcoxon signed rank test (*$P < 0.05$).

DEVELOPMENT OF THE IFC-BASED CBMN ASSAY PROTOCOL FOR THE RABiT-II SYSTEM

The challenge to adapt the IFC-based CBMN assay protocol for the RABiT-II system was that the robotic platform uses 96-well plates with a maximum working volume of 250 µl per well, including blood and media. Furthermore, it has been recommended that at least 200 BNCs should be scored in the CBMN assay for triage radiation biodosimetry (27, 28). Therefore, to adapt the IFC-based CBMN method for the automated RABiT-II system, we further modified the sample processing protocol and data acquisition and analysis templates to increase the BNC yield-per-culture volume and improve the accuracy of BNC and MN identification.

Blood-to-Media Ratio

To ensure that the maximum number of BNCs would be generated within the limited culture volume of 250 µl, we tested blood-to-media ratios. Figure 2A shows a comparison of dose-response curves obtained from 100 µl of blood cultured in 900 µl of PB-MAX media (blood-to-media ratio 1:9) with 200 µl of blood cultured in 800 µl of PB-MAX media (blood-to-media ratio 2:8) using the 96-well 1.4 ml Matrix tube format described above (n = 4 donors). Coefficients for the dose-response calibration curves are shown in Table 1. The results show that the mean MN frequency for both the 1:9 and 2:8 blood-to-media conditions was similar, indicating that increasing the blood-to-media ratio did not adversely affect MN frequency. Furthermore, due to the increased blood volume, the total number of BNCs is generally higher from the 2:8 ratio than the 1:9 ratio in samples with the same total culture volume across the 0–4 Gy dose range. On average, 544 BNCs were obtained from the 2:8 ratio while only 300 BNCs were captured from the 1:9 ratio, an improvement of 81%. Statistical significance was tested using the Wilcoxon signed rank test, with differences between the two data points at 0, 1 and 2 Gy being statistically significant ($P < 0.05$). As such, it was decided that a blood-to-media ratio of 2:8 would be used for all subsequent experiments.

Addition of Hypotonic Solution

The effect of increasing the blood-to-media ratio resulted in an increase in partially lysed RBCs and apoptotic/necrotic cell debris (data not shown), which hindered the acquisition of isolated BNC images and impacted the accuracy of MN quantification. The most effective strategy to improve RBC lysis, while maintaining a simple processing method, is through the addition of a hypotonic solution step (75 mM KCl, 800 µl) to whole blood prior to FLS (2, 29). Figure 3A shows that in addition to improving RBC lysis and eliminating the apoptotic/necrotic cell debris, 75 mM KCl caused the lymphocytes to swell slightly prior to fixation. This improved the circular morphology of, and separation between, the main nuclei. In addition, the DRAQ5 staining was much more uniform in the main nuclei and the MN. The MN were also better separated from the main nuclei, and therefore easier to mask in IDEAS. Figure 3B shows the MN dose-response calibration curves generated from samples processed in the presence and absence of KCl. The inclusion of KCl reduced nonirradiated, baseline MN levels by 51% (0.055 ± 0.012 to 0.028 ± 0.014) and at the lower doses, removed many of the dim artifacts resulting from non-uniform DRAQ5 staining, which were close to the main nuclei that were incorrectly scored as MN (28, 30). Furthermore, R^2 values improved from 0.70 to 0.87 (Table 1).

DRAQ5 Concentration

High-quality staining of the BNCs and MN is critical for their capture using the ISX and accurate identification in IDEAS. DRAQ5 was determined to be the best DNA dye for IFC-based CBMN assay with 488-nm laser (21),
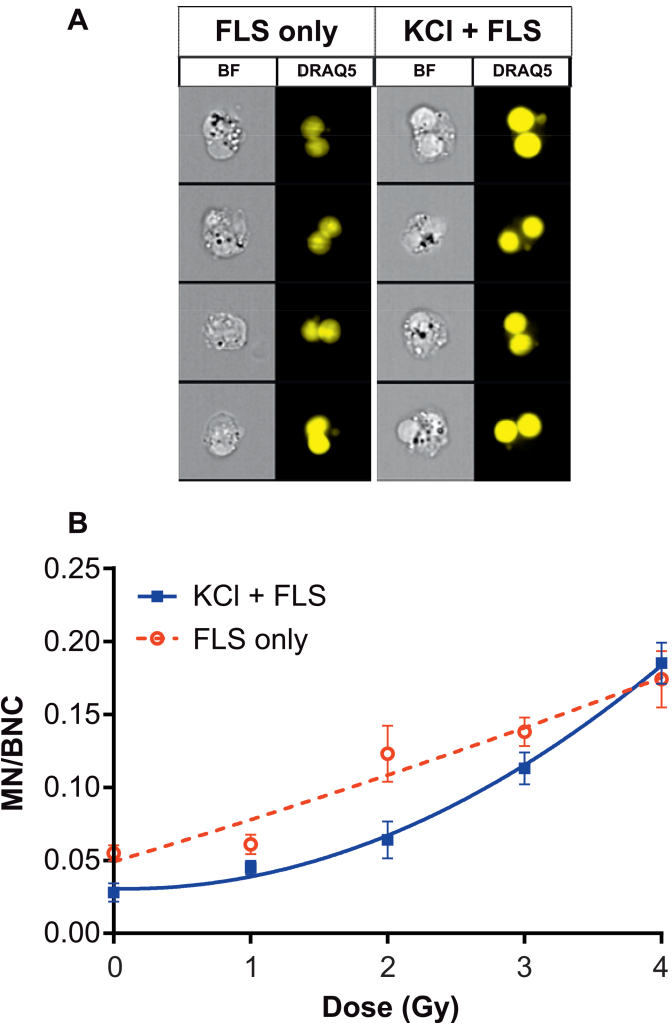
A

B

FIG. 3. Improvements to the BNC images and dose-response calibration curves through the addition of hypotonic solution (75 m*M* KCl). Panel A: More spatially separated nuclei and MN, with more uniform DRAQ5 staining intensity was observed with the use of KCl. Panel B: The dose-response calibration curves representing the average of four donors showing the rate of MN/BNC using sample processing protocols with or without the use of KCl. Error bars represent the standard error of the mean.

A

B

FIG. 4. Improvement in the MN and BNC images through the optimization of DRAQ5 concentration. Panel A: At 20 μ*M* of DRAQ5, the BNC images demonstrate optimal signal-to-noise ratio. Panel B: Average dose-response calibration curves for four different donors using either 10, 20 or 50 μ*M* as the final concentration of DRAQ5. Error bars represent the standard error of the mean.

however, the optimal concentration of the dye has not been examined. If the staining is too dim, low-intensity fluorescent artifacts can be incorrectly identified as MN. Conversely, if the staining is too bright, the main nuclei can appear blurred or saturated and the number of legitimate BNCs will be underestimated. This also increases the chances that very bright artifacts can be incorrectly identified as MN. Thus, it was essential to determine the optimal concentration of DRAQ5.

Figure 4A demonstrates that samples stained with only 10 μ*M* DRAQ5 showed relatively low fluorescent intensity in the two main nuclei and were not being correctly identified in IDEAS. Furthermore, a number of dim artifacts were incorrectly identified as MN, as evidenced by overestimation of the 0 Gy MN frequencies and high standard errors (Fig. 4B). In contrast, samples stained with 50 μ*M* DRAQ5
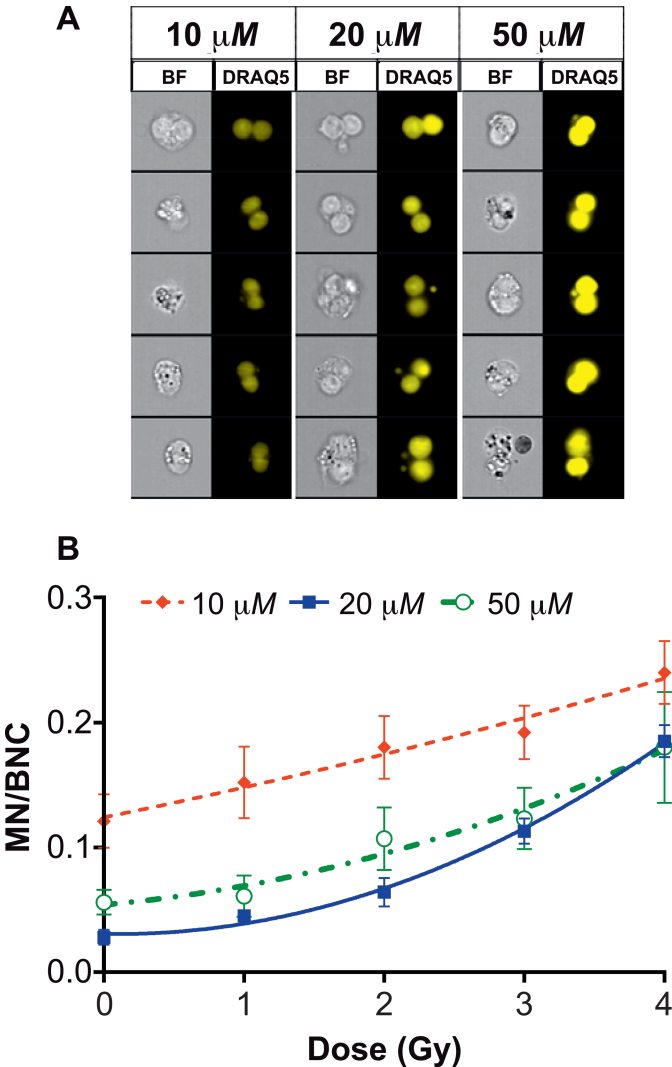
exhibited overstaining and saturation of the BNCs and MN, resulting in a number of bright artifacts at the edges of the nuclei being incorrectly identified as MN, most noticeably at 0 Gy (Fig. 4B). Overall, the data confirmed that at 20 μ*M* DRAQ5, the main nuclei and MN were more uniformly stained, leading to a better signal-to-noise ratio and identification of MN, resulting in an improved linear-quadratic dose-response calibration curve (Table 1).

Optimization of Data Acquisition on ISX

To further optimize the assay for small volume and increase the throughput of the assay, we modified the acquisition template to improve the efficiency of data collection on the ISX. A template was created that permitted rejection of a number of undesired events such as doublets,
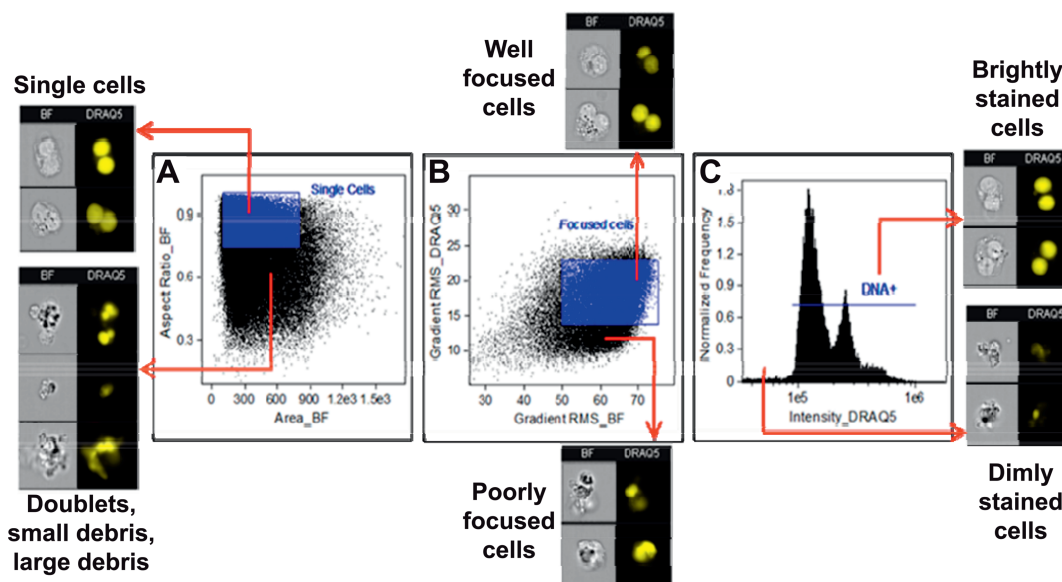
FIG. 5. Data acquisition template used to collect only single, highly-focused, DNA-positive cells. Panel A: Bivariate plot of BF aspect ratio versus BF area, allowing for the selection of single cells and the removal of doublets and small and large debris. Panel B: Bivariate plot of DRAQ5 gradient RMS versus BF gradient RMS enabling the selection of sharply-focused cells while eliminating blurry cells. Panel C: Histogram of DRAQ5 intensity allows for the selection of DNA positive cells and the elimination of very dimly stained cells.

large aggregates, unfocused nuclear images and very dimly stained cells. This ensured that all data files contained mostly sharply focused, single cell images. Figure 5 shows the sequential application of each region that was applied during acquisition along with representative imagery. This optimization of the data acquisition template reduced the total number of collected events from 200,000 to approximately 30,000 while maintaining the same number of single cells collected. Previously, by only gating out very small debris, data file sizes reached up to 2 GB. By using the gating strategy described here during acquisition, data file sizes were reduced to approximately 300 MB, on average, which in turn, reduced the average analysis time per file in IDEAS by 78%, from 9 min to 2 min.

Optimization of the Analysis Template in IDEAS

To ensure that the IDEAS analysis template was performing correctly with the improvements made to the sample processing methodology, all images in the final BNC and MN populations were visually inspected. It was observed that some artifacts residing outside of the cytoplasm and between the two nuclei, as well as some dim and elongated artifacts, were being incorrectly scored as MN. Therefore, we added two additional panels in the IDEAS template (Fig. 6) to eliminate these false-positive MNs.

In IDEAS, by using masks to highlight specific pixels in regions of interest and then using features to perform calculations based on those masks, certain attributes of the image can be quantified, such as area, aspect ratio, among others. Figure 6A shows how artifacts residing outside the cytoplasm or between the two nuclei are eliminated. A mask was created on the BF images to identify the cytoplasm of the cell (Fig. 6A, top image) and the distance between this mask and the MN mask was calculated using the Spot Distance feature. Distances greater than zero indicated that the MN resided outside of the cytoplasm. Next, to remove artifacts between the two nuclei, the skeleton mask, which highlights pixels along the center of the semi-major axis of the image, was created on the BNC image (Fig. 6A, middle image). If the distance between this mask and the MN mask was equal to zero, this indicated that the spot identified by the MN mask was actually an artifact between the two nuclei. Figure 6B shows how dim and elongated artifacts that are incorrectly identified as true MN were eliminated. The aspect ratio provides a measure of circularity, and objects with an aspect ratio of less than 0.45 were observed to be elongated artifacts (Fig. 6B, bottom image). The ratio of the median pixel values of both the BNC and MN masks was calculated, and potential MN that had a median pixel intensity less than one fourth of the median pixel intensity of the BNC mask were determined to be dim artifacts (Fig. 6B, top image). A region was then created that allowed for the exclusion of both of these false-positive events from MN (Fig. 6B, middle image). Finally, visual inspection of the BNC population containing MN before and after addition of the new panels in the template revealed that the false-positive rate of MN was reduced by 20% based on previous observations, from 15% (*24*) to 12%.
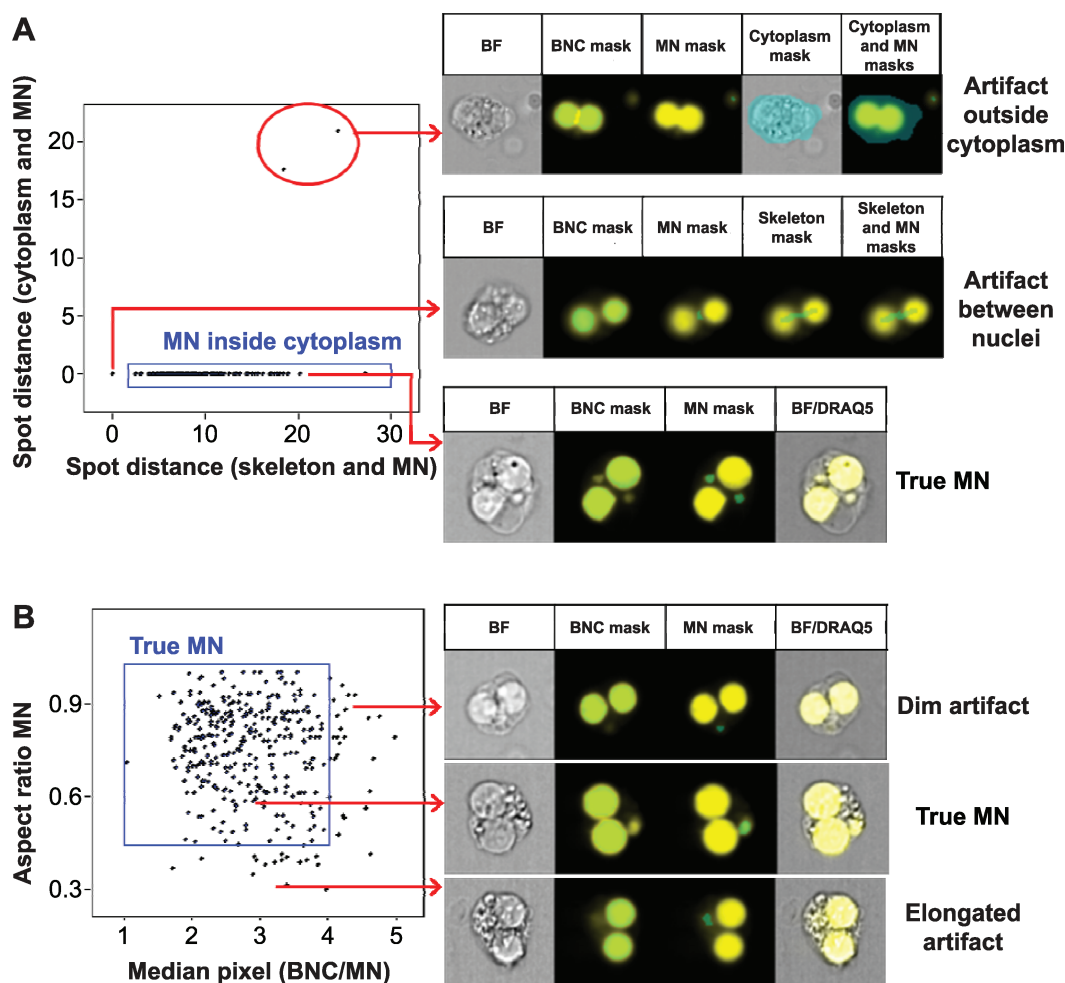
FIG. 6. Elimination of false positive artifacts. Panel A: Use of the cytoplasm mask to identify false-positive MN residing outside of the cytoplasm (top image) and the skeleton mask to identify artifacts residing between the two nuclei that are incorrectly identified as MN (middle image). Panel B: Use of the aspect ratio of the MN mask to identify elongated false-positive MN and the ratio of the median pixel intensity of the MN and BNC images to eliminate dim artifacts.

INTEGRATION OF THE OPTIMIZED IFC-CBMN PROTOCOL INTO THE RABiT-II

Based on these modifications to the sample preparation protocol and the data acquisition and analysis templates, we cultured 50 µl of blood with 200 µl of media in 96-well plates (Corning® Inc., Corning, NY) and harvested the samples using the RABiT-II cell::explorer system (PerkinElmer® Inc., Waltham, MA).

Whole blood samples (1 ml) from six health donors were irradiated up to 4 Gy as described previously. Aliquots of 50 µl per irradiated blood samples were dispensed to wells containing 200 µl PB-MAX karyotyping media in the 96-well plate. Each well was mixed five times using a multi-channel pipet. Plates were incubated in an STX500 automated incubator (LiCONiC US Inc., Woburn, MA), maintained in a humidified environment at 37°C, 5% CO_2. After 24 h of incubation, Cyto-B was added to cultures at a final concentration of 6 µg/ml. Figure 7A shows the blood sample processing protocol for RABiT-IFC CBMN assay by combining the RABiT-II cell::explorer with the ISX.

At the end of culture, the plate cover was removed by a robotic arm (Denso Inc., Long Beach, CA) and centrifuged by a V-Spin 96-well plate centrifuge (Agilent Technologies, Santa Clara, CA). All centrifugations were performed at 250g for 2 min. The supernatant was removed from each well using an EL406e microplate washer (BioTek® Instruments, Winooski, VT).

As with most high-throughput/high-content screening (HTS/HCS) systems, the cell::explorer consists of sub-stations surrounding the anthropomorphic robotic arm (*12*). After centrifugation and aspiration, several steps were performed automatically by the system on all samples:

1. 160 µl of hypotonic solution (75 m*M* KCl) was added by FlexDrop™ (PerkinElmer) modules, mixed thoroughly using JANUS platform (PerkinElmer) and samples were incubated at room temperature for 10 min. After this, 40
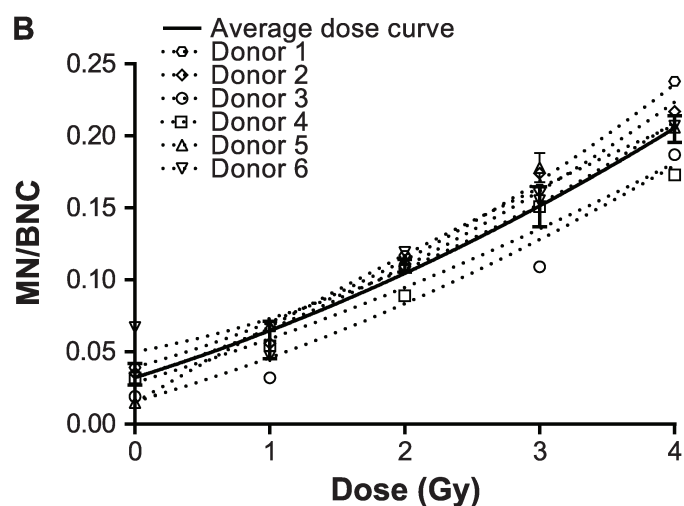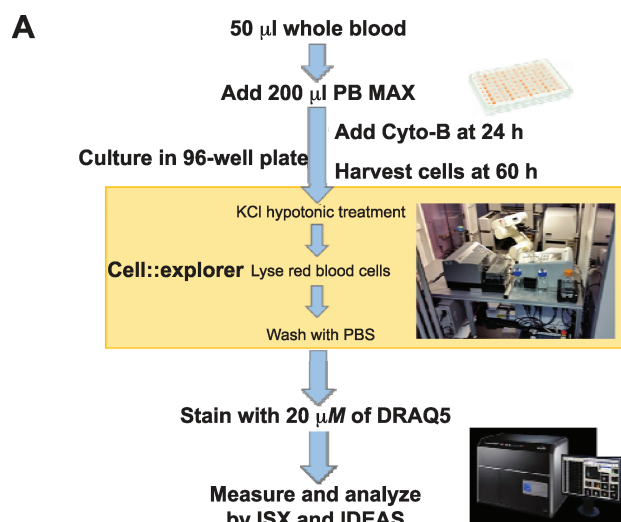
A

B

FIG. 7. Automated CBMN assay combining the RABiT-II and ISX systems using 50 μl-whole blood samples. Panel A: Final protocol for sample processing. Panel B: Individual dose-response curves showing the rate of MN per BNC in γ-ray irradiated human lymphocytes. Dashed lines represent the rate of MN per BNC versus dose of each individual donor. The solid line represents average rate of MN per BNC versus dose from all six healthy donors. Each curve was fitted with a separate liner-quadratic function.

TABLE 2
Average Number of Binucleated Cells (BNCs), Rate of MN/BNC and Data Collection Time for the RABiT-IFC CBMN Assay Using 50 μl of Whole Blood

Dose (Gy)	Collection time (min)	Total events	BNCs	MN/BNC
0	10.8	26,203	452	0.032
1	13.1	22,927	284	0.058
2	12.5	25,916	306	0.110
3	12.1	24,378	296	0.149
4	12.5	26,507	288	0.202

On average, more than 200 BNCs were acquired at each dose from each donor within approximately 13 min on ISX (Table 2). Dose-response calibration curves showing the rate of MN per BNC from six donors is shown in Fig. 7B and coefficient values calculated for each linear-quadratic fit as well as the goodness of fit (R^2) from all calibration curves are shown in Table 3.

DISCUSSION AND CONCLUSIONS

The CBMN assay is a well-established technique that has been shown to provide accurate dose estimates after exposure to ionizing radiation (2). Automation plays an important role in this assay to allow for unbiased sample processing and data acquisition (30). Recently, we have developed the RABiT-II based on the IN Cell Analyzer (11, 12), a commercial imaging system used to measure the MN frequency in irradiated human blood lymphocytes using fingerstick-sized samples (12). The current article describes the integration of high-throughput IFC technology into our robotic RABiT-II workstation. The development of an automated end-to-end RABiT-IFC CBMN assay could potentially improve the "time to result" for triage radiation biodosimetry.

To adapt the IFC-based CBMN protocol for the RABiT-II system, we modified the existing methods into a 96-well format. Given that the RABiT-II system only uses 96-well plates, with a maximum working volume to 250 μl per sample, the challenge here was to develop a small-volume protocol that could generate more than 200 BNCs after irradiation, a requirement for dose estimation (27). To this end, we increased the blood-to-media ratio, added hypotonic solution to remove RBC debris and improve the circular nuclear morphology of BNCs and MN, and optimized the DRAQ5 concentration to ensure more uniform nuclear staining, all of which increased the yield of BNCs per culture. To improve MN identification, we further modified the image-processing algorithms within the IDEAS software. New masks and features were created using both BF and DRAQ5 imagery to avoid incorrectly identifying DNA-positive artifacts as MN. This is advantageous as BF images of the cell can be used to ensure that the main nuclei and MN are contained within the same cell,

μl of FLS was added using the FlexDrop modules and samples were centrifuged.

2. Any remaining RBCs were lysed through the addition of 200 μl of FLS using FlexDrop modules, mixed thoroughly using JANUS platform and incubated at room temperature for 15 min.

3. Cells were washed 3 times with PBS by 96-well plate centrifuge and supernatant was removed by the microplate washer. DRAQ5 was then added to all fixed samples at final concentration of 20 μM, incubated for 5 min and transferred to the ISX for image acquisition and analysis.

TABLE 3
Coefficient and Goodness of Fit (R²) Values Calculated for Each Linear-Quadratic Calibration Curve for the RABiT-IFC CBMN Assay Using 50 μl of Whole Blood

	$\beta \pm SE$	$\alpha \pm SE$	$c \pm SE$	R^2
Donor 1	$(5.9 \pm 0.2) \times 10^3$	$(21.6 \pm 0.9) \times 10^3$	$(43.8 \pm 0.8) \times 10^3$	0.93
Donor 2	$(6.5 \pm 0.2) \times 10^3$	$(20.8 \pm 0.7) \times 10^3$	$(31.9 \pm 0.4) \times 10^3$	0.82
Donor 3	$(4.2 \pm 0.4) \times 10^3$	$(0.1 \pm 1.7) \times 10^3$	$(16.0 \pm 1.1) \times 10^3$	0.79
Donor 4	$(3.7 \pm 0.4) \times 10^3$	$(2.14 \pm 1.4) \times 10^3$	$(31.9 \pm 1.1) \times 10^3$	0.83
Donor 5	$(0.1 \pm 0.6) \times 10^3$	$(53.8 \pm 2.5) \times 10^3$	$(15.0 \pm 2.0) \times 10^3$	0.85
Donor 6	$(7.0 \pm 0.5) \times 10^3$	$(13.2 \pm 2.2) \times 10^3$	$(42.6 \pm 2.2) \times 10^3$	0.84
Average	$(4.1 \pm 2.4) \times 10^3$	$(26.3 \pm 10.2) \times 10^3$	$(30.5 \pm 8.5) \times 10^3$	0.89

which is currently not possible with other imaging systems such as the Metafer™ (*31*).

These modifications have allowed us to successfully integrate automated high-throughput image capture capabilities of IFC into our robotic RABiT-II workstation. Overall, we have increased the throughput of the CBMN assay and shortened the ''time to result'' by optimizing the sample preparation protocols and integrating these two systems using only 50 μl of blood sample. Automated preparation of a full plate of 96 samples for using the RABiT-II workstation can be completed within 1 h from the end of the cell culture to the fixed samples resuspended in PBS. Thus, sample preparation throughput using the RABiT-II approach with a full 96-well plate has the potential to process approximately 2,300 samples in a 24-h period. Additionally, by optimizing the data acquisition on the ISX to eliminate unnecessary events and reduce the data file size, we have also reduced data acquisition and analysis time to approximately 15 min per sample. Finally, linear-quadratic dose calibration curves up to 4 Gy from six healthy donors were generated from automatically scoring more than 200 BNCs per 50 μl blood. These curves demonstrate that the system is able to identify increases in MN frequency with increasing dose up to 4 Gy.

There are several benefits of applying IFC to perform the CBMN assay, such as the elimination of slide-making, which represents a major bottleneck in triage radiation biodosimetry. Additionally, IFC is capable of acquiring cellular imagery at high flow rates, reaching up to 1,000 events per s, making it comparable to, or faster than other automated scoring techniques such as the Metafer platform (*31*). Moreover, IFC is capable of capturing images from both nuclear staining and whole cell morphology using the BF. This permits visual validation of all acquired images as well as automated analysis using mathematical algorithms in IDEAS. The enhanced analysis presented here has improved the accuracy of the assay by avoiding the scoring of MN or other DNA positive debris outside the cell. There are, however, a number of limitations with current IFC technology. We have reported a lower magnitude of MN frequency (approximately 20%) at 4 Gy in this study, when compared with results from manual microscopy, which is consistent with MN frequencies reported in other work using IFC (*23, 24*). The discrepancy between the two

methods can likely be attributed to the fact that images obtained by IFC are 2D projections of a 3D cell, which may cause some MN to be hidden behind the main nucleus or to reside at a depth of focus different from the main nuclei. Future technical advances in IFC to obtain 3D imagery may provide a solution to these issues.

In summary, we have successfully integrated the ISX imaging flow cytometer into our RABiT-II system, resulting in a fully automated end-to-end RABiT-IFC CBMN assay using fingerstick-sized blood samples. This methodology presented here has the potential to increase capacity for triage radiation biodosimetry response. Future studies will aim to validate this assay to ensure accuracy in dose prediction, facilitating its application in a large-scale radiological/nuclear event.

REFERENCES

1. Fenech M, Morley AA. Measurement of micronuclei in lymphocytes. Mutat Res 1985; 147:29–36.
2. Fenech M. Cytokinesis-block micronucleus cytome assay. Nat Protoc 2007; 2:1084–104.
3. Fenech M, Morley AA. Cytokinesis-block micronucleus method in human lymphocytes: effect of in vivo ageing and low dose X-irradiation. Mutat Res 1986; 161:193–8.
4. Fenech M. The lymphocyte cytokinesis-block micronucleus cytome assay and its application in radiation biodosimetry. Health Phys 2010; 98:234–43.
5. Fenech M. The in vitro micronucleus technique. Mutat Res Fund Mol Mech Mut 2000; 455:81–95.
6. Schunck C, Johannes T, Varga D, Lorch T, Plesch A. New developments in automated cytogenetic imaging: unattended scoring of dicentric chromosomes, micronuclei, single cell gel electrophoresis, and fluorescence signals. Cytogenet Genome Res 2004; 104:383–89.
7. Varga D, Johannes T, Jainta S, Schuster S, Schwarz-Boeger U,

Kiechle M, et al. An automated scoring procedure for the micronucleus test by image analysis. Mutagenesis 2004; 19:391–97.

8. Willems P, August L, Slabbert J, Romm H, Oestreicher U, Thierens H, et al. Automated micronucleus (MN) scoring for population triage in case of large scale radiation events. Int J Radiat Biol 2010; 86:2–11.

9. Garty G, Turner HC, Salerno A, Bertucci A, Zhang J, Chen Y, et al. The decade of the rabit (2005–15). Radiat Prot Dosimetry 2016; 172:201–06.

10. Garty G, Chen YH, Turner HC, Zhang J, Lyulko OV, Bertucci A, et al. The RABiT: a rapid automated biodosimetry tool for radiological triage. II. technological developments. Int J Radiat Biol 2011; 87:776–90.

11. Garty G, Chen YH, Salerno A, Turner H, Zhang J, Lyulko O, et al. The RABIT: a rapid automated biodosimetry tool for radiological triage. Health Phys 2010; 98:209–17.

12. Repin M, Pampou S, Karan C, Brenner DJ, Garty G. RABiT-II: Implementation of a high-throughput micronucleus biodosimetry assay on commercial biotech robotic systems. Radiat Res 2017; 187:492–98.

13. Lyulko OV, Garty G, Randers-Pehrson G, Turner HC, Szolca B, Brenner DJ. Fast image analysis for the micronucleus assay in a fully automated high-throughput biodosimetry system. Radiat Res 2014; 181:146–61.

14. Turner HC, Brenner DJ, Chen Y, Bertucci A, Zhang J, Wang H, et al. Adapting the gamma-H2AX assay for automated processing in human lymphocytes. 1. Technological aspects. Radiat Res 2011; 175:282–90.

15. Turner HC, Sharma P, Perrier JR, Bertucci A, Smilenov L, Johnson G, et al. The RABiT: High-throughput technology for assessing global DSB repair. Radiat Environ Biophys 2014; 53:265–72.

16. Sharma PM, Ponnaiya B, Taveras M, Shuryak I, Turner H, Brenner DJ. High throughput measurement of gammaH2AX DSB repair kinetics in a healthy human population. PLoS One 2015; 10:e0121083.

17. Repin M, Turner HC, Garty G, Brenner DJ. Next generation platforms for high-throughput biodosimetry. Radiat Prot Dosimetry 2014; 159:105–10.

18. Basiji DA. Principles of Amnis imaging flow cytometry. Methods Mol Biol 2016; 1389:13–21.

19. Rodrigues MA. Automation of the in vitro micronucleus assay using the Imagestream® imaging flow cytometer. Cytometry Part A 2018; 93:706–26.

20. Rodrigues MA, Beaton-Green LA, Wilkins RC, Fenech MF. The potential for complete automated scoring of the cytokinesis block micronucleus cytome assay using imaging flow cytometry. Mutat Res 2018; 836:53–64.

21. Rodrigues MA, Beaton-Green LA, Kutzner BC, Wilkins RC. Automated analysis of the cytokinesis-block micronucleus assay for radiation biodosimetry using imaging flow cytometry. Radiat Environ Biophys 2014; 53:273–82.

22. Rodrigues MA, Beaton-Green LA, Kutzner BC, Wilkins RC. Multi-parameter dose estimations in radiation biodosimetry using the automated cytokinesis-block micronucleus assay with imaging flow cytometry. Cytometry A 2014; 85A:883–93.

23. Rodrigues MA, Beaton-Green LA, Wilkins RC. Validation of the cytokinesis-block micronucleus assay using imaging flow cytometry for high throughput radiation biodosimetry. Health Phys 2016; 110:29–36.

24. Rodrigues MA, Probst CE, Beaton-Green LA, Wilkins RC. Optimized automated data analysis for the cytokinesis-block micronucleus assay using imaging flow cytometry for high throughput radiation biodosimetry. Cytometry A 2016; 89:653–62.

25. Rodrigues MA, Probst CE, Beaton-Green LA, Wilkins RC. The effect of an optimized imaging flow cytometry analysis template on sample throughput in the reduced culture cytokinesis-block micronucleus assay. Radiat Prot Dosimetry 2016; 172:223–9.

26. Fenech M, Chang WP, Kirsch-Volders M, Holland N, Bonassi S, Zeiger E. HUMN project: detailed description of the scoring criteria for the cytokinesis-block micronucleus assay using isolated human lymphocyte cultures. Mutat Res Genet Toxicol Environ Mutagen 2003; 534:65–75.

27. Cytogenetic dosimetry: applications in preparedness for and response to radiation emergencies. Emergency Preparedness and Response. Vienna: International Atomic Energy Agency; 2011. (https://bit.ly/2FTE47h)

28. McNamee JP, Flegal FN, Greene HB, Marro L, Wilkins RC. Validation of the cytokinesis-block micronucleus (CBMN) assay for use as a triage biological dosimetry tool. Radiat Prot Dosimetry 2009; 135:232–42.

29. Yamamoto M, Motegi A, Seki J, Miyamae Y. The optimized conditions for the in vitro micronucleus (MN) test procedures using chamber slides. Environ Mutagen Res 2005; 27:145–51.

30. Fenech M, Kirsch-Volders M, Rossnerovac A, Sram R, Romm H, Bolognesi C, et al. HUMN project initiative and review of validation, quality control and prospects for further development of automated micronucleus assays using image cytometry systems. Int J Hyg Environ Health 2013; 216:541–52.

31. Seager AL, Shah U-K, Brusehafer K, Wills J, Manshian B, Chapman KE, et al. Recommendations, evaluation and validation of a semi-automated, fluorescent-based scoring protocol for micronucleus testing in human cells. Mutagenesis 2014; 29:155–64.